

Absorption spectrum of doped highly mismatched alloys

Hassan Allami

Department of Physics, University of Ottawa, Ottawa, ON K1N 6N5, Canada

Jacob J. Krich

*Department of Physics, University of Ottawa, Ottawa, ON K1N 6N5, Canada and
School of Electrical Engineering and Computer Science,
University of Ottawa, Ottawa, ON K1N 6N5, Canada*

Highly mismatched alloys (HMA's) are a class of semiconductor alloys with large electronegativity differences between the alloying elements. We predict the absorption spectrum due to transitions between the split bands of a doped highly mismatched alloy with a conduction band anticrossing. We analyze the joint densities of states for both direct and indirect transitions between the split bands. The resulting spectrum has features that reveal the unusual state distribution that is characteristic of HMAs, hence providing valuable insight into their electronic structure. In particular, we predict a peak near the absorption edge, which arises due to the suppression of direct transitions at large momenta. We present analytic forms for the near-absorption-edge and large-energy spectra, showing that they are qualitatively different from those in standard parabolic semiconductors. In particular, as a result of suppressed direct transitions, indirect transitions dominate the spectrum away from the edge of absorption.

I. INTRODUCTION

Semiconductor alloys where the electronegativity or size of the alloying elements significantly differs are called highly mismatched alloys (HMA's). The hallmark of HMA's, as in the prototypical case of GaAsN, is a bandgap that changes with alloying in a way that cannot be explained with a simple bowing parameter [1], a feature that found many applications in making various optoelectronic devices [2, 3]. According to the band anticrossing (BAC) model, the large decrease in the valence-to-conduction band gap with alloying is associated with a second band gap that opens between two split bands E_- and E_+ . According to the BAC, these split bands represent the hybridization of localized states from the alloying element with the conduction band of the host semiconductor (See Fig. 1) [4]. When the localized states hybridize with a single conduction band (CB) of the host, the gap opens by splitting the CB into two split bands, E_- and E_+ . In such HMA's with a CB anticrossing, the splitting can generate a narrow intermediate band, E_- , in the original bandgap of the host. The presence of the narrow band makes HMA's a candidate for implementing intermediate band solar cells [5–11], which have the potential to break the Shockley-Queisser limit on solar cell efficiency [12]. Going beyond the BAC, the HMA electronic structure has unusual properties distinct from standard semiconductors [13], which can manifest in their plasmonic properties when doped [14].

Although the absorption spectrum between the two split bands of an HMA is crucial for operating such intermediate band solar cells, there is not much known about it. While there has been success in doping HMA's so the E_- band is partially full at equilibrium [15], the absorption spectra of doped HMA's have not been studied. The optical absorption of such doped systems is a powerful tool for studying their band structure, which will add

to our growing knowledge of these alloys [16].

In this work, we predict the absorption spectra of doped highly mismatched alloys with a conduction band anticrossing. We predict the qualitative features of the E_- to E_+ HMA absorption spectrum by calculating the direct and indirect joint densities of states of the system. We show how these spectra reflect the special electronic structure that arises from the hybridization of localized states with band states, which is distinct in physics and in absorption signatures from absorption in standard semiconductors. The characteristic predicted signature is a visible peak near the edge of absorption, which is distinguishable from a possible excitonic peak. We focus on the case of ZnCdTeO to illustrate these phenomena and their qualitative features.

II. ABSORPTION SPECTRUM AND JOINT DENSITY OF STATES

While the BAC model [4] is very successful in describing the energy levels in the band structure of HMA's, it is quiet about how the propagating states are distributed among these energies. The average Green's function introduced by Wu et al. [13] captures this special aspect of state distribution in HMA's. Here, building on their average Green's function, we show how the special state distribution should lead to qualitative features in the absorption spectrum of doped HMA's.

A. HMA's special distribution of states and the absorptivity

According to the BAC model [4], large differences in the electronegativities of the mismatched elements compared to the host leads to the formation of localized states

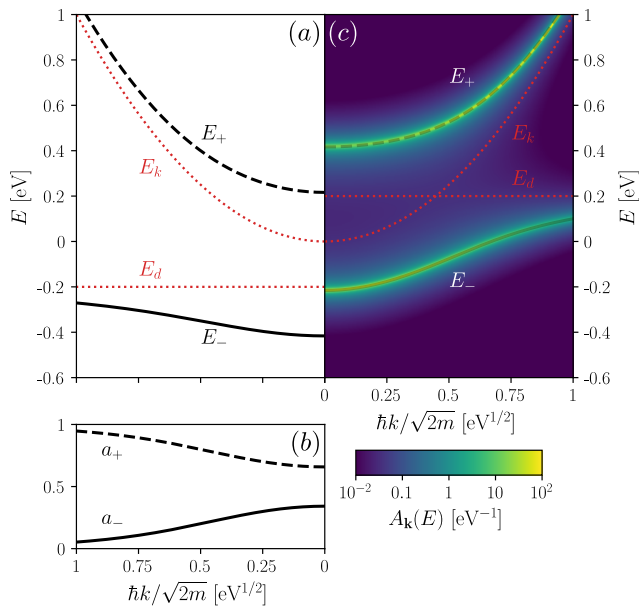


FIG. 1. (a) Band anticrossing bands E_{\pm} according to Eq. (1), and (b) their corresponding spectral weighting factors a_{\pm} from Eq. (10), with defect energy $E_d = -0.2$ eV and broadening $\Gamma = 0$. (c) Spectral density $A_{\mathbf{k}}(E)$ for $E_d = 0.2$ eV and $\Gamma = 100$ meV from Eq. (6). Note the logarithmic colorscale. For reference, E_{\pm} according to Eq. (1) are also plotted in (c). In both cases $V = 3$ eV and $x = 1\%$.

with energy E_d . These localized states hybridize with the propagating states of the unalloyed host, which have dispersion $E_{\mathbf{k}}$, resulting in the emergence of two new split bands with dispersions

$$E_{\pm} = \frac{1}{2} \left(E_{\mathbf{k}} + E_d \pm \sqrt{(E_{\mathbf{k}} - E_d)^2 + 4V^2x} \right), \quad (1)$$

where V is the coupling energy between the localized and the propagating states, and x is the alloy fraction of the mismatching element (see Fig. 1).

Although Eq. (1) is a great approximation for the energy dispersion of E_{\pm} , the split bands of HMA's are not just two regular bands arising from a periodic potential of a crystal. They are both offspring of the hybridization of a single band with a series of randomly distributed localized states. If we assume that the alloying elements are uniformly distributed, as in the coherent potential approximation [17], we may still use the crystal momentum \mathbf{k} as a good quantum number in an ensemble-average sense. The exact hybridized eigenstates with energy E have a non-zero projection on each \mathbf{k} state. As a result, at each \mathbf{k} , there is a distribution $A_{\mathbf{k}}(E)$, known as the spectral density, that describes the projection of all hybridized states with energy E on the \mathbf{k} states. As we show in Section II B, the spectral density $A_{\mathbf{k}}(E)$ can be broken into two branches, $A_{\mathbf{k}}^{\pm}(E)$, corresponding to E_{\pm} .

Now consider a doped HMA where some excess electrons are occupying the E_{\pm} bands. Under illumination

with radiation of frequency ω , suppose we want to calculate transition rates of electrons from E_- -energy states to E_+ -energy states. In standard semiconductors, the strongest transitions are direct, conserving \mathbf{k} between initial and final states. To find the direct transition amplitudes, at each \mathbf{k} we must know how many states there are in each band. For example, the density of spin up electrons at \mathbf{k} belonging to the E_- band is $\int dE A_{\mathbf{k}}^-(E) f_E$, instead of the usual $f_{E_-}(\mathbf{k})$, where $f_E = (e^{(E-\mu)/T} + 1)^{-1}$ is the Fermi distribution at temperature T and chemical potential μ .

Standard discussion of absorptivity in semiconductors begins from a Fermi's golden rule analysis, generally called the Kubo-Greenwood formula [18]. The absorptivity for photons with energy E is controlled most importantly by the joint density of states (jDOS) at energy E , which describes the number of pairs of states in the lower-energy and higher-energy bands that are separated by energy E . Calculating the jDOS, we need to take $A_{\mathbf{k}}$ into account, as it carries important information about the special state distribution of HMA's. For direct absorption processes, the relevant jDOS is $D_j(E)$, which includes only pairs of states with the same momentum \mathbf{k} . For indirect absorption processes, the relevant jDOS is $\rho_j(E)$, which includes all pairs of states separated by energy E , regardless of \mathbf{k} . For both contributions to the optical absorption, there is a matrix element that must be averaged over all contributing initial and final states. The result is that the absorptivity due to direct processes $\alpha_d \propto |M_D|^2 D_j(E)/E$ and the absorptivity due to indirect processes $\alpha_i \propto |M_{\rho}|^2 \rho_j(E)/E$, where M_D and M_{ρ} are the averaged matrix elements.

We consider both direct momentum-conserving transitions between E_- and E_+ and indirect transitions that do not conserve momentum. Indirect transitions are typically made possible through phonon exchange, but in the case of an alloy are also possible without phonons, due to the disorder. Absorption and emission of phonons that make the indirect transitions possible bring a small shift to the edge of the optical absorption spectrum, which we neglect as it does not affect the qualitative features we describe here. Neglecting the energy dependence of the matrix elements and the phonon energy shift [18], we have

$$\alpha(E) \propto \frac{D_j(E) + v\rho_j(E)}{E}, \quad (2)$$

where $v = |M_{\rho}|^2/|M_D|^2$ is a volume scale of the system, which we treat as a free parameter.

Calculating the jDOS's for HMA's must account for the distribution of electrons at different energies according to $A_{\mathbf{k}}^{\pm}(E)$. So, we write the direct and indirect jDOS

as

$$D_j(E) = \frac{1}{\mathcal{V}} \int dE_1 dE_2 \sum_{\mathbf{k}} A_{\mathbf{k}}^-(E_1) A_{\mathbf{k}}^+(E_2) f_{E_1} (1 - f_{E_2}) \delta(E_2 - E_1 - E), \quad (3)$$

$$\rho_j(E) = \frac{1}{\mathcal{V}^2} \int dE_1 dE_2 \sum_{\mathbf{k}\mathbf{k}'} A_{\mathbf{k}}^-(E_1) A_{\mathbf{k}'}^+(E_2) f_{E_1} (1 - f_{E_2}) \delta(E_2 - E_1 - E), \quad (4)$$

where \mathcal{V} is the volume of the system. Comparing the dimension of Eq. (3) and Eq. (4) also shows why the ratio $v = |M_\rho|^2 / |M_D|^2$ has the dimension of volume. Note that we neglect the spin degree of freedom – unless otherwise mentioned – as it does not affect the shape of $\alpha(E)$. The presence of $A_{\mathbf{k}}^\pm$ in the jDOS expressions produces the signatures of the special state distribution of E_\pm in the absorption spectrum of a doped HMA.

B. HMA spectral density and resulting joint density of states

We now discuss how the special distribution of states in HMA's, given by $A_{\mathbf{k}}(E)$, generates special features in α according to Eq. (2). We begin by deriving $A_{\mathbf{k}}(E)$.

Based on Anderson's impurity model [19], Wu et al. built an average Green's function for electrons in the conduction bands of an HMA [13]

$$G(E, \mathbf{k}) = \left[E - E_{\mathbf{k}} - \frac{V^2 x}{E - E_d + i\Gamma} \right]^{-1}, \quad (5)$$

which successfully recovers the spectrum of the BAC model. The new parameter $\Gamma = \pi\beta V^2 \rho_0(E_d)$ determines the broadening of the Green's function's spectral density, where ρ_0 is the unperturbed density of propagating states in a unit cell and has dimension of inverse energy. In what follows we consider a generic case where $E_{\mathbf{k}}$ is a parabolic conduction band and all energies are measured from its edge. Therefore, for instance, $\Gamma \rightarrow 0$ for $E_d < 0$, as $\rho_0 = 0$ below the conduction band edge.

While Eq. (5) and the BAC model contain the same energy spectrum in the limit that $\Gamma \rightarrow 0$, even in that limit the spectral density $A_{\mathbf{k}}(E) = -\text{Im}[G(E, \mathbf{k})]/\pi$ contains information about what fraction of an electron can be in each of the states. Since there is less than one alloying atom per unit cell of the host crystal, the E_- and E_+ bands can not each hold as many electrons as the original $E_{\mathbf{k}}$ band.

We can divide $A_{\mathbf{k}}(E)$ into two pieces, corresponding to E_\pm as

$$A_{\mathbf{k}}(E) = A_{\mathbf{k}}^+(E) + A_{\mathbf{k}}^-(E) = \frac{1}{\pi} \sum_{s=\pm} \text{Im} \left[\frac{\tilde{a}_s}{E - \tilde{E}_s} \right], \quad (6)$$

where, including the effects of Γ , the dispersion of Eq. (1) is generalized to

$$\tilde{E}_\pm = \frac{1}{2} \left(E_{\mathbf{k}} + \tilde{E}_d \pm \sqrt{(E_{\mathbf{k}} - \tilde{E}_d)^2 + 4V^2 x} \right), \quad (7)$$

with $\tilde{E}_d = E_d + i\Gamma$, and the generalized weight factors are

$$\tilde{a}_\pm = \pm \frac{V^2 x}{(\tilde{E}_+ - \tilde{E}_-)(\tilde{E}_\pm - E_{\mathbf{k}})}. \quad (8)$$

A realization of $A_{\mathbf{k}}(E)$ with a finite Γ is shown in Fig. 1(c). Note that most of the spectral weight is near the BAC bands, but the weight spreads out to nearby energies, as well.

When $\Gamma \rightarrow 0$, Eq. (7) reduces to Eq. (1) and the spectral density reduces to two delta functions at E_\pm

$$\lim_{\Gamma \rightarrow 0} A_{\mathbf{k}}(E) = a_+ \delta(E - E_+) + a_- \delta(E - E_-), \quad (9)$$

with

$$a_\pm = \pm \frac{V^2 x}{(E_+ - E_-)(E_\pm - E_{\mathbf{k}})}, \quad (10)$$

which we derived previously to show how the state distribution in HMA's affects their plasmonic properties [14]. The weight factors a_\pm in Eq. (10) are positive numbers smaller than 1, representing the share of a single \mathbf{k} state in each of E_\pm . A realization of a_\pm is shown in Fig. 1(b) in a case with $E_d < 0$ where $\Gamma \rightarrow 0$.

In the limit $\Gamma \rightarrow 0$, we can find analytic forms for Eqs. (3,4). These results are exact for the $E_d < 0$ case. While the analytic forms are not exact when $E_d > 0$, the analytic results from the $\Gamma \rightarrow 0$ limit provide useful insight to the behavior of D_j and ρ_j with finite Γ as well. We derive these analytic forms and their implications for finite Γ cases in Appendix A. Table I summarizes the qualitative results, showing the scaling of D_j and ρ_j with energy near their respective energy onset and at large energy.

The most significant prediction is that the direct E_- to E_+ optical transition is suppressed at higher energy, where the BAC bands alone would predict that transitions should still be present. The E_- states at high k have mostly localized character, and as a result the spectral density a_- is small, as is visible in Fig. 1. Since there is little weight in these large- k states, $D_j(E)$ is suppressed, producing a peak in the direct optical absorption spectrum. In particular, as we show in Appendix A, $D_j \sim E^{-3/2}$ for large E , as opposed to the usual \sqrt{E} behavior in direct-gap parabolic semiconductors. Further $\rho_j \sim \sqrt{E}$, as opposed to E^2 behavior in indirect parabolic semiconductors. Note that the jDOS for transitions from an isolated defect to a parabolic band also shows \sqrt{E} behavior, as it mimics the single-particle DOS of the receiving band (see Table I).

The presence of the peak in the direct optical absorption is our main prediction, and according to Eq. (2) should be visible in plots of $E\alpha(E)$. Ordinary parabolic semiconductors do not show a similar qualitative feature from their direct band-to-band absorption. As we show in the Appendix A, the width of the peak is controlled by $|E_d|$ when $E_d < 0$ and by Γ when $E_d > 0$. Hence this

TABLE I. Asymptotic behavior of D_j and ρ_j in $\Gamma \rightarrow 0$ limit at the absorption edge and for large E . The two cases of negative and positive E_d are compared with a semiconductor with parabolic bands. E_D is the edge of direct transitions, and E_ρ is the edge of indirect transitions. The edge behavior of D_j and ρ_j is discussed in Appendix A.

	D_j		ρ_j	
	Edge	Large E	Edge	Large E
$E_d < 0$ HMA	$\sqrt{E - E_D}$	$E^{-3/2}$	$E - E_\rho$	\sqrt{E}
$E_d > 0$ HMA	$1/\sqrt{E - E_D}$	$E^{-3/2}$	$E - E_\rho$	\sqrt{E}
parabolic semiconductor	$\sqrt{E - E_D}$	\sqrt{E}	$(E - E_\rho)^2$	E^2

peak also provides a practical way to estimate Γ , which is otherwise a difficult quantity to measure.

We do not know the ratio of indirect to direct matrix elements v , but in general in semiconductors indirect processes are weaker than direct ones, as they need to couple phonons in to the system. However, since HMA's are random alloys and not crystalline semiconductors, it is possible that momentum conservation between states holds less strongly than in standard semiconductors, which would elevate the indirect ρ_j contribution with respect to the direct D_j contribution to the absorption spectrum. Indirect processes are most important at energies where the direct processes are forbidden, and we predict the form of the E_- to E_+ absorption spectrum assuming the same pattern will hold. We predict that since D_j decays as $E^{-3/2}$ for large E , while ρ_j grows as \sqrt{E} , then if v is large enough the indirect transitions will dominate the large- E part of the E_- to E_+ absorption spectrum. Ref. 9 on the transient absorption spectrum of HMA's invoked indirect transitions to explain their observed high-energy absorption. Here we provide a firm theoretical basis for indirect transitions dominating direct transitions at higher energy. The indirect absorption edge occurs at lower energy than the direct absorption edge, allowing indirect absorption also to dominate for energies below the direct absorption edge. This effect is most noticeable when $E_d < 0$, since the direct absorption spectrum is broadened by Γ when $E_d > 0$.

All of these features are the direct consequence of the special distribution of states in HMA's, and detecting them in experiments would be a good validation test for the theory.

III. EXPERIMENTAL SIGNATURES

We illustrate the predictions for the signatures of E_- to E_+ optical absorption by considering HMA's from the ZnCdTeO family, where the BAC parameters have been estimated [20, 21]. $\text{Zn}_{1-y}\text{Cd}_y\text{Te}_{1-x}\text{O}_x$ is a II-VI quaternary HMA in which ZnCdTe forms the standard semiconductor and oxygen plays the role of mismatching element.

TABLE II. Parameters of BAC model for $\text{Zn}_{1-y}\text{Cd}_y\text{Te}_{1-x}\text{O}_x$ [20, 21], where m_e is the free electron mass.

Parameters	$y = 0$	$y = 1$
E_d [eV]	-0.27	0.38
V [eV]	2.8	2.2
m [m_e]	0.117	0.09

It has been the subject of extensive studies and used as an HMA of choice in making devices [8, 15, 20, 22–26]. We choose ZnCdTeO for our case study because there have been successful attempts in doping the E_- band with chlorine donors [15]. Moreover, controlling the Cd concentration allows for sweeping E_d . BAC parameters for the ternary endpoint alloys are given in Table II, which shows that by increasing Cd fraction, E_d moves from negative to positive. For the sake of demonstration we show the results for the two ternary endpoints, ZnTeO and CdTeO, but tuning to the Cd fraction allows realization of any E_d between -0.27 and 0.38 eV, along with changes in V and m , as shown in Table II.

In parabolic band semiconductors, $\alpha(E)$ shows a peak due to the factor of E in the denominator of Eq. (2). Instead, we consider $E\alpha$ to detect the unusual peak of doped HMA's. While experimentally we generally specify doping level n , the absorption depends most directly on the chemical potential appearing in the Fermi function f_E . We relate them using

$$n = \frac{2}{v} \int dE \sum_{\mathbf{k}} A_{\mathbf{k}}(E) f_E, \quad (11)$$

where the factor of 2 accounts for spin degeneracy. In Fig. 2 we plot $E\alpha$ at $T = 300$ K for doped ZnTeO (top) and CdTeO (bottom), according to Eq. (2), for two doping levels. For the case with a lower doping level, we also show the contributions of direct and indirect transitions to $E\alpha$ separately (shaded blue). We use $v = 10 \text{ nm}^3$, chosen strong enough so that ρ_j visibly dominates D_j away from the edge of absorption. To calculate D_j and ρ_j for CdTeO we used the full form in Eqs. (3,4). For ZnTeO, since $E_d < 0$ and $\Gamma \rightarrow 0$, we use Eq. (A2) to compute D_j and Eq. (A4) to calculate ρ_j .

The absorption peak from the direct transitions is clear for both materials in Fig. 2. We can see that the CdTeO ($E_d > 0$) peak is narrower than the one in ZnTeO ($E_d < 0$), which we expect as the $E_d > 0$ cases have peak widths controlled by Γ while the $E_d < 0$ have them controlled by $|E_d|$, as discussed in Appendix A. And since $\Gamma \propto \sqrt{E_d}$ when $E_d > 0$, we expect to see narrower peaks for cases with smaller $|E_d|$.

Figure 2 also demonstrates that the indirect transitions dominate at large E in both material systems, due to the decaying large- E tail of D_j . Also, the indirect transitions become available at lower energy – as they are not limited by conservation of momentum – but this effect is only visible for the $E_d < 0$ case where $\Gamma \rightarrow 0$ doesn't smear

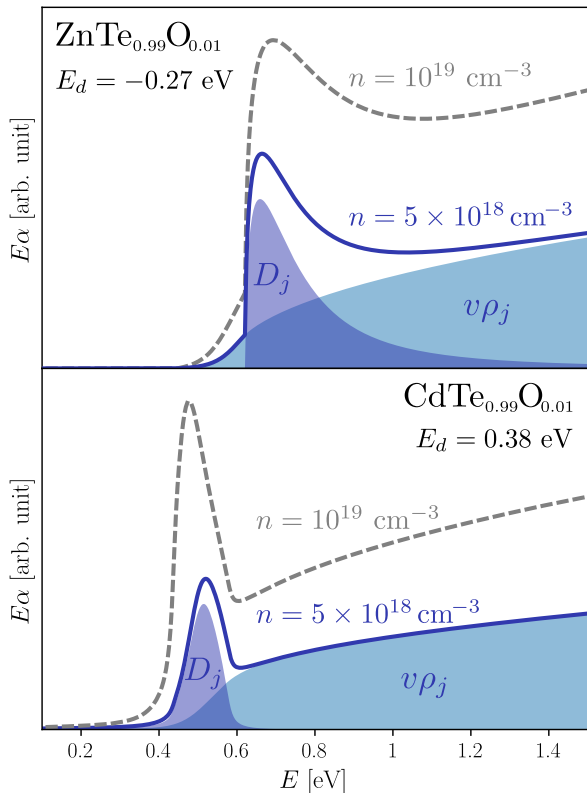


FIG. 2. E_- to E_+ optical absorption $E\alpha$ at $T = 300$ K for ZnCdTeO alloys with two doping levels, $n = 5 \times 10^{18} \text{ cm}^{-3}$ (solid blue), and $n = 10^{19} \text{ cm}^{-3}$ (dashed grey). The separate contributions of direct and indirect transitions also shown for the lower doping level (shaded blue), according to Eq. (2), where $v = 10 \text{ nm}^3$ is used for all cases. (top) $\text{ZnTe}_{1-x}\text{O}_x$, with $x = 1\%$, and BAC parameters listed in Table II, for which $\Gamma \rightarrow 0$. (bottom) $\text{CdTe}_{1-x}\text{O}_x$, with $x = 1\%$, BAC parameters listed in Table II, and $\Gamma = 10 \text{ meV}$ for broadening.

out the edge of absorption. Since Γ being zero in the $E_d < 0$ case gives sharper features to α , we also expect the edge of D_j to be visible as a kink in the absorption in these cases, as shown for ZnTeO.

To show the effects of increased filling of the E_- band, we include two doping levels in Fig. 2, $n = 5 \times 10^{18} \text{ cm}^{-3}$

(solid blue), and $n = 10^{19} \text{ cm}^{-3}$ (dashed grey), for both ZnTeO and CdTeO. It is clear that the special features of $E\alpha$ – the absorption peak and the domination of indirect transitions at large E – are present at both doping levels. It is possible that excitonic peaks, which generally occur at energies just below the jDOS onset [27], could be confused for the peak that we predict. The evolution of the peak as a result of increasing doping also provides a way to distinguish it from a possible excitonic peak. In a doped HMA, both screening from carriers in the E_- band and the disordered potential should suppress excitons [28], so we expect the possible excitonic peak to diminish at higher doping. As Fig. 2 shows, the peak that we expect to be visible in $E\alpha$ naturally grows stronger at higher doping, making it distinguishable from an excitonic one.

It is worth noting that although according to Ref. 15 achieving chlorine concentration up to and even higher than 10^{20} cm^{-3} is possible, it is not clear what portion of the dopants are electrically active. Especially as our model with weighted bands shows, E_- has a relatively small maximum capacity for carrying excess electrons. For instance, for $\text{ZnTe}_{1-x}\text{O}_x$ and $\text{CdTe}_{1-x}\text{O}_x$ with $x = 1\%$ used for plotting Fig. 2, the maximum capacity of E_- is about $5 \times 10^{19} \text{ cm}^{-3}$ and $6 \times 10^{19} \text{ cm}^{-3}$ respectively. Electrically active doping above those levels will populate the E_+ band, with changes to the E_- to E_+ absorption spectrum, similar to the Moss-Burstein shift [29, 30].

In the ZnCdTeO system, the typical frequency range for E_- to E_+ absorption is around 0.1 – 1 eV, or a wavelength of 1 – 10 microns. These spectra can be observed with FTIR or other techniques appropriate for these long wavelengths. We look forward to seeing the results of such experiments, to see if they confirm our theoretical predictions. We believe experimental results for the absorption spectrum of doped HMA's will be instrumental in understanding their interesting electronic structure better.

ACKNOWLEDGMENTS

We acknowledge funding from the NSERC CREATE TOP-SET program, Award Number 497981.

Appendix A: Analytic forms and asymptotics of D_j and ρ_j

1. Direct joint density of states

Using the sharp $A_{\mathbf{k}}$ in Eq. (9), the E_1 and E_2 integrals in Eq. (3) become trivial. Furthermore, since $E_{\mathbf{k}} = \hbar^2 k^2 / 2m$ is isotropic we can integrate the angles out to obtain a 1-dimensional integral

$$D_j(E) = \frac{1}{V} \sum_{\mathbf{k}} a_- a_+ f_{E_-} (1 - f_{E_+}) \delta(E_+ - E_- - E) = \frac{V^2 x}{2\pi^2} \int_0^\infty \frac{f_{E_-} (1 - f_{E_+})}{(E_+ - E_-)^2} \delta(E_+ - E_- - E) k^2 dk. \quad (\text{A1})$$

Note that the factor of $a_- a_+$ originates from the nontrivial spectral density of the HMA, and this extra factor produces the $(E_+ - E_-)^2$ in the denominator of Eq. (A1), which makes D_j decay for large E , instead of following the standard \sqrt{E} behavior in parabolic semiconductors.

When $E_d \leq 0$, $E_+ - E_-$ has a minimum at $k = 0$ with the value $\sqrt{E_d^2 + 4V^2x}$. Therefore, the argument of the delta function in Eq. (A1) has a zero if $E \geq \sqrt{E_d^2 + 4V^2x}$, determining the edge of D_j . Carrying out the delta function integral is straightforward and gives

$$D_j(E) = \left(\frac{2m}{\hbar^2}\right)^{3/2} \frac{V^2x\sqrt{E_d + \sqrt{E^2 - 4V^2x}}}{4\pi^2E\sqrt{E^2 - 4V^2x}} f_{\hat{E}_-} (1 - f_{\hat{E}_+}) \Theta\left(E - \sqrt{E_d^2 + 4V^2x}\right), \quad (\text{A2})$$

where $\hat{E}_\pm = E_d + \frac{1}{2}(\sqrt{E^2 - 4V^2x} \pm E)$, and Θ is the unit step function. One can see that the fraction in Eq. (A2) decays as $E^{-3/2}$ for large E (see Table I). Since D_j in Eq. (A2) is positive, continuous, and zero at the edge of direct transitions $E_D = \sqrt{E_d^2 + 4V^2x}$, it must have a peak. The width of that peak is determined by $|E_d|$. In this case, $D_j(E)$ rises as $\sqrt{E - E_D}$, the same as the direct joint density in parabolic semiconductors (see Table I). The peak is visible in the top panel of Fig. 2, which is plotted for an HMA with $E_d < 0$.

When $E_d > 0$, $E_+ - E_-$ has a minimum at $k = \sqrt{2mE_d}/\hbar$ with value $2V\sqrt{x}$, which leads to a van Hove singularity at $E_D = 2V\sqrt{x}$ with the same form as the van Hove singularities in 1D materials with parabolic bands. That is, for $E \geq E_D$, $D_j(E) \sim 1/\sqrt{E - E_D}$, which is divergent at the onset. This 1D-like form arises from the finite k^2 volume element when $E_+ - E_-$ reaches its minimum value in Eq. (A1). The van Hove singularity arises only when $A_{\mathbf{k}}$ is sharp as in Eq. (9), in the limit of $\Gamma \rightarrow 0$ (see Table I). But when $E_d > 0$, Γ is non-zero and broadens $A_{\mathbf{k}}^\pm$. Finite Γ turns the divergence of D_j into a peak with a width determined by Γ . The peak is visible in the bottom panel of Fig. 2, which shows an HMA with $E_d > 0$.

The other consequence of $E_+ - E_-$ having a minimum at finite k is that the argument of the delta function in Eq. (A1) has two zeros when $2V\sqrt{x} < E < \sqrt{E_d^2 + 4V^2x}$, which leads to two separate contributions to the integral. However, for large E , where the finite Γ effect is also unimportant, there is only one contribution to the integral in Eq. (A1). Therefore, the large E behavior of D_j is the same for both positive and negative E_d (see Table I).

2. Indirect joint density of states

To evaluate the non- k -conserving density of states in Eq. (4), it is helpful to first find the single-particle density of states in each band $\rho_\pm(E)$ by performing \mathbf{k}, \mathbf{k}' integrals. In the sharp case, where $A_{\mathbf{k}}$ is given by Eq. (9), we can separately define the densities in each band

$$\rho_\pm(E) = \frac{1}{V} \sum_{\mathbf{k}} a_\pm \delta(E - E_\pm) = \frac{1}{4\pi^2} \left(\frac{2m}{\hbar^2}\right)^{3/2} \begin{cases} \sqrt{E - \frac{V^2x}{E - E_d}} & \text{for } E \text{ in } E_\pm \\ 0 & \text{otherwise,} \end{cases} \quad (\text{A3})$$

where we used Eq. (10) for a_\pm . Integrating \mathbf{k}, \mathbf{k}' out in Eq. (4) we obtain

$$\rho_j(E) = \int dE_1 dE_2 \rho_-(E_1) \rho_+(E_2) f_{E_1} (1 - f_{E_2}) \delta(E_2 - E_1 - E) = \int dE_1 \rho_-(E_1) \rho_+(E_1 + E) f_{E_1} (1 - f_{E_1 + E}). \quad (\text{A4})$$

The edge of ρ_j is at the minimum gap between the E_+ and E_- bands, given by $E_\rho = \frac{1}{2}(\sqrt{E_d^2 + 4V^2x} - E_d)$, and it rises linearly (see Table I). In the limit of large E , the E -dependence in Eq. (A4) comes from ρ_+ , which goes as \sqrt{E} , as can be seen from Eq. (A3). Therefore, ρ_j shows \sqrt{E} behavior for large E , which is different from the standard E^2 behavior in semiconductors with parabolic bands (see Table I). The more important implication of this result is that since D_j decays as $E^{-3/2}$, the indirect transitions can dominate the large- E part of the E_- to E_+ absorption spectrum, where the direct transitions are suppressed. Fig. 2 shows this effect away from the edge of absorption.

Lastly, we note that non-zero Γ smears out the edge of ρ_j and has no significant effect on its large- E behavior.

[1] M. Weyers, M. Sato, and H. Ando, Red shift of photoluminescence and absorption in dilute GaAsN alloy layers,

Jpn. J. Appl. Phys. **31**, L853 (1992).

[2] S. Nakamura and M. R. Krames, History of gallium-

- nitride-based light-emitting diodes for illumination, *Proc. IEEE* **101**, 2211 (2013).
- [3] D. Friedman, J. Geisz, S. Kurtz, and J. Olson, 1-eV solar cells with GaInNAs active layer, *J. Cryst. Growth* **195**, 409 (1998).
- [4] W. Shan, W. Walukiewicz, J. W. Ager, E. E. Haller, J. F. Geisz, D. J. Friedman, J. M. Olson, and S. R. Kurtz, Band anticrossing in GaInNAs alloys, *Phys. Rev. Lett.* **82**, 1221 (1999).
- [5] N. López, L. A. Reichertz, K. M. Yu, K. Campman, and W. Walukiewicz, Engineering the electronic band structure for multiband solar cells, *Phys. Rev. Lett.* **106**, 028701 (2011).
- [6] N. Ahsan, N. Miyashita, M. M. Islam, K. M. Yu, W. Walukiewicz, and Y. Okada, Two-photon excitation in an intermediate band solar cell structure, *Appl. Phys. Lett.* **100**, 172111 (2012).
- [7] M. Welna, M. Baranowski, W. M. Linhart, R. Kudrawiec, K. M. Yu, M. Mayer, and W. Walukiewicz, Multicolor emission from intermediate band semiconductor $\text{ZnO}_{1-x}\text{Se}_x$, *Sci. Rep.* **7**, 44214 (2017).
- [8] T. Tanaka, K. M. Yu, Y. Okano, S. Tsutsumi, S. Haraguchi, K. Saito, Q. Guo, M. Nishio, and W. Walukiewicz, Improved open-circuit voltage and photovoltaic properties of ZnTeO-based intermediate band solar cells with n-type ZnS layers, *IEEE J. Photovolt.* **7**, 1024 (2017).
- [9] J. N. Heyman, A. M. Schwartzberg, K. M. Yu, A. V. Luce, O. D. Dubon, Y. J. Kuang, C. W. Tu, and W. Walukiewicz, Carrier lifetimes in a III-V-N intermediate-band semiconductor, *Phys. Rev. Appl.* **7**, 014016 (2017).
- [10] K. Zelazna, R. Kudrawiec, A. Luce, K.-M. Yu, Y. J. Kuang, C. W. Tu, and W. Walukiewicz, Photorefectance studies of optical transitions in GaNPAs intermediate band solar cell absorbers, *Sol. Energy Mater. Sol. Cells* **188**, 99 (2018).
- [11] J. N. Heyman, E. M. Weiss, J. R. Rollag, K. M. Yu, O. D. Dubon, Y. J. Kuang, C. W. Tu, and W. Walukiewicz, THz transient photoconductivity of the III-V dilute nitride $\text{GaP}_y\text{As}_{1-y-x}\text{N}_x$, *Semicond. Sci. Technol., Semicond. Sci. Technol.* **33**, 125009 (2018).
- [12] A. Luque and A. Martí, Increasing the efficiency of ideal solar cells by photon induced transitions at intermediate levels, *Phys. Rev. Lett.* **78**, 5014 (1997).
- [13] J. Wu, W. Walukiewicz, and E. E. Haller, Band structure of highly mismatched semiconductor alloys: Coherent potential approximation, *Phys. Rev. B* **65**, 233210 (2002).
- [14] H. Allami and J. J. Krich, Plasma frequency in doped highly mismatched alloys, *Phys. Rev. B* **103**, 035201 (2021).
- [15] T. Tanaka, K. Matsuo, K. Saito, Q. Guo, T. Tayagaki, K. M. Yu, and W. Walukiewicz, Cl-doping effect in $\text{ZnTe}_{1-x}\text{O}_x$ highly mismatched alloys for intermediate band solar cells, *J. Appl. Phys.* **125**, 243109 (2019).
- [16] W. Walukiewicz and J. M. O. Zide, Highly mismatched semiconductor alloys: From atoms to devices, *J. Appl. Phys.* **127**, 010401 (2020).
- [17] R. J. Elliott, J. A. Krumhansl, and P. L. Leath, The theory and properties of randomly disordered crystals and related physical systems, *Rev. Mod. Phys.* **46**, 465 (1974).
- [18] M. P. Marder, Optical properties of semiconductors, in *Condensed Matter Physics* (John Wiley & Sons, Ltd, 2010) Chap. 21, pp. 633–657.
- [19] P. W. Anderson, Localized magnetic states in metals, *Phys. Rev.* **124**, 41 (1961).
- [20] T. Tanaka, K. Mizoguchi, T. Terasawa, Y. Okano, K. Saito, Q. Guo, M. Nishio, K. M. Yu, and W. Walukiewicz, Compositional dependence of optical transition energies in highly mismatched $\text{Zn}_{1-x}\text{Cd}_x\text{Te}_{1-y}\text{O}_y$ alloys, *Appl. Phys. Express* **9**, 021202 (2016).
- [21] S. Adachi, *Properties of Semiconductor Alloys: Group-IV, III-V and II-VI Semiconductors* (John Wiley & Sons, 2005) Chap. 7, p. 150.
- [22] T. Tanaka, Y. Nagao, T. Mochinaga, K. Saito, Q. Guo, M. Nishio, K. M. Yu, and W. Walukiewicz, Molecular beam epitaxial growth of ZnCdTeO epilayers for intermediate band solar cells, *J. Cryst. Growth* **378**, 259 (2013).
- [23] T. Tanaka, M. Miyabara, Y. Nagao, K. Saito, Q. Guo, M. Nishio, K. M. Yu, and W. Walukiewicz, Photocurrent induced by two-photon excitation in ZnTeO intermediate band solar cells, *Appl. Phys. Lett.* **102**, 052111 (2013).
- [24] T. Tanaka, S. Kusaba, T. Mochinaga, K. Saito, Q. Guo, M. Nishio, K. M. Yu, and W. Walukiewicz, Molecular beam epitaxial growth and optical properties of highly mismatched $\text{ZnTe}_{1-x}\text{O}_x$ alloys, *Appl. Phys. Lett.* **100**, 011905 (2012).
- [25] M. Welna, R. Kudrawiec, Y. Nabetani, T. Tanaka, M. Jaquez, O. D. Dubon, K. M. Yu, and W. Walukiewicz, Effects of a semiconductor matrix on the band anticrossing in dilute group II-VI oxides, *Semicond. Sci. Technol.* **30**, 085018 (2015).
- [26] M. Welna, L. Janicki, W. M. Linhart, T. Tanaka, K. M. Yu, R. Kudrawiec, and W. Walukiewicz, Effects of the host conduction band energy on the electronic band structure of ZnCdTeO dilute oxide alloys, *J. Appl. Phys.* **126**, 083106 (2019).
- [27] D. C. Reynolds and T. C. Collins, *Excitons: Their Properties and Uses* (Elsevier, 2012).
- [28] V. L. Bonch-Bruевич and V. D. Iskra, On the theory of the Wannier-Mott excitons in disordered semiconductors, *Phys. Status Solidi B* **68**, 369 (1975).
- [29] E. Burstein, Anomalous optical absorption limit in InSb, *Phys. Rev.* **93**, 632 (1954).
- [30] T. S. Moss, The interpretation of the properties of indium antimonide, *Proc. Phys. Soc. B* **67**, 775 (1954).